Title

Plasmonic nanoreactors regulating selective oxidation by energetic electrons and nanoconfined thermal fields

Journal

Science Advances, 7(10)

ISSN

2375-2548

Authors

Zhan, Chao
Wang, Qiu-Xiang
Yi, Jun
et al.

Publication Date

2021-03-05

DOI

10.1126/sciadv.abf0962

Peer reviewed

CHEMISTRY

Plasmonic nanoreactors regulating selective oxidation by energetic electrons and nanoconfined thermal fields

Chao Zhan[1], Qiu-Xiang Wang[1], Jun Yi[1], Liang Chen[1], De-Yin Wu[1], Ye Wang[1], Zhao-Xiong Xie[1]*, Martin Moskovits[1,2]*, Zhong-Qun Tian[1]*

Optimizing product selectivity and conversion efficiency are primary goals in catalysis. However, efficiency and selectivity are often mutually antagonistic, so that high selectivity is accompanied by low efficiency and vice versa. Also, just increasing the temperature is very unlikely to change the reaction pathway. Here, by constructing hierarchical plasmonic nanoreactors, we show that nanoconfined thermal fields and energetic electrons, a combination of attributes that coexist almost uniquely in plasmonic nanostructures, can overcome the antagonism by regulating selectivity and promoting conversion rate concurrently. For propylene partial oxidation, they drive chemical reactions by not only regulating parallel reaction pathways to selectively produce acrolein but also reducing consecutive process to inhibit the overoxidation to CO_2, resulting in valuable products different from thermal catalysis. This suggests a strategy to rationally use plasmonic nanostructures to optimize chemical processes, thereby achieving high yield with high selectivity at lower temperature under visible light illumination.

INTRODUCTION

The ideal catalytic process efficiently produces desired target products with little or no undesirable side products under the cost-effective set of conditions, although this ideal condition is rarely achieved because high efficiency and high selectivity are often antagonistic goals. Using partial oxidation as an example, a relatively high temperature is necessary to overcome the large barrier of oxygen activation, thereby achieving high reactant conversion (*1*, *2*). However, increasing the operating temperature of the environment normally leads to notable quantities of overoxidized and, therefore, undesirable products (*2*, *3*). Thus, a compromise must be made between selectivity and efficiency. High temperatures also have other undesirable consequences, such as a decreased catalyst lifetime, leading to higher cost and longer downtimes (*4*, *5*). Moreover, just increasing the temperature is very unlikely to regulate the reaction pathway. A given molecule usually requires different catalysts to generate different products, and each catalyst has different efficiency and selectivity performances.

Surface plasmons (SPs) can act to redistribute photons, electrons, and heat energy in time and space (*6*–*9*). Numerous recent demonstrations have stimulated current research activity and suggest that plasmonic nanostructures can lead to light-driven chemistry carried out under milder conditions than thermal catalysis (*10*–*18*). These processes make use of one or both of the two main consequences of the relaxation of SPs, energetic electrons and local heating (*19*–*24*), thereby increasing the rates of chemical reactions (details are shown in fig. S1). SPs have been proposed as promising approaches to facilitate chemical reactions (*8*, *20*, *21*, *23*, *25*–*28*). For example, oxygen activation is accelerated on illuminated plasmonic nanostructures, where the energetic electrons and local heating are the drivers (*29*–*31*). Also, SP-induced energetic electrons are reported to drive chemical reactions in nanolocalized regions (*32*–*34*). However, the observed improvement provided by SPs has been primarily on conversion. Although recent studies have attempted to address the challenge of using SPs to regulate the catalytic selectivity (*11*, *35*, *36*), our understanding of the mutual effects on selectivity and conversion efficiency of the reaction is still limited, especially when the reaction happens in the nanoconfined plasmonic reactor with energetic electrons and heating. Different from other nanoreactors confined by materials such as nanocages, nanotubes, or nanopores, plasmonic nanoreactors are generated by confining electromagnetic and thermal fields in open space. Also, such nanoconfined fields in plasmonic nanoreactors are inhomogeneous with great gradient, which may have distinctively different effect on physical and chemical processes.

Here, using propylene (PE) partial oxidation as a model system and a plasmonic hierarchical nanostructure as catalyst, we show that the excitation of SPs is able to simultaneously improve selectivity and conversion efficiency, thereby simultaneously achieving high yields of acrolein or propylene oxide (PO) with high selectivity at low operating temperatures. The catalyst consists of well-defined Cu_2O nanocrystals, which, on their own, have good catalytic activity and are further activated by plasmonic gold nanoparticles (NPs) (*37*–*39*). Under visible light illumination, the propylene conversion was found to increase approximately 18-fold, while the selectivity of acrolein concurrently increased from approximately 50 to 80%, and the overoxidation was greatly inhibited. Such outcomes cannot be achieved using a thermal stimulus alone. By varying the wavelength and intensity of the incident light, using SiO_2 shells to isolate the electronic effects, and developing a computational model to help us understand the ongoing processes, we systematically determined how plasmonic effects, including energetic electrons and nanoconfined thermal fields, enable these chemical processes. Moreover, energetic electrons and nanoconfined thermal fields have different effects on reaction selectivity, corresponding to regulate the reaction pathway to selectively produce acrolein or eliminate consecutive reactions to increase the selectivity of all partial oxidation products.

[1]State Key Laboratory of Physical Chemistry of Solid Surfaces, College of Chemistry and Chemical Engineering, Collaborative Innovation Center of Chemistry for Energy Materials (iChEM), Xiamen University, Xiamen 361005, China. [2]Department of Chemistry, University of California, Santa Barbara, Santa Barbara, CA 93106, USA.
*Corresponding author. Email: zqtian@xmu.edu.cn (Z.-Q.T.); moskovits@chem.ucsb.edu (M.M.); zxxie@xmu.edu.cn (Z.-X.X.)

RESULTS

Characterization of catalysts and their catalytic performance response to illumination

Partial oxidation of propylene was carried out in a quartz microreactor at atmospheric pressure, allowing simultaneous temperature control and illumination (fig. S2). This reaction was chosen, in part, on account of its great commercial value (*40*). In addition, it contains both the parallel and consecutive reaction processes (Fig. 1A) on Cu-based catalysts (*37*), including at least the α-H bond oxidation to acrolein (P1) and the carbon-carbon double bond oxidation to PO (P2), and both of the partial oxidation products continued to oxidize to CO_2. Also, the various partial oxidation products generated have been associated with specific active oxygen species. For example, lattice oxygen species are thought to preferentially oxidize the reactive allylic hydrogen atoms, while epoxidation makes use of an electrophilic oxygen (*3*, *41*). The output of a 300-W xenon lamp, filtered to exclude the ultraviolet region, was used as light source with a total intensity of 200 mW/cm^2. The reaction gas was a mixture of 13.3% C_3H_6 and 6.7% O_2 in helium, flowing at 50 ml/min. Acrolein, PO, and carbon dioxide were identified as the dominant reaction products (details are given in Materials and Methods). Uniform cubic Cu_2O (C-Cu_2O) nanocrystals without surfactant were synthesized using the reported methods (*39*). The surface of the as-prepared C-Cu_2O is smooth and exposes only (100) faces, 300 to 500 nm in size (fig. S3). Gold NPs with diameters of ~30 nm (figs. S4 and S5) were assembled on the C-Cu_2O (100) faces to form the hierarchical catalyst shown in Fig. 1B (figs. S6 and S7). The gold NPs showed no catalytic activity under experimental conditions (fig. S8). X-ray diffraction (XRD) and x-ray photoelectron spectroscopy (XPS) confirmed that the crystal structure and surface composition of the C-Cu_2O did not change after loading with gold NPs (Fig. 1, C and D, and figs. S9 to S14).

Figure 1E shows the steady-state conversion and selectivity of propylene oxidation using the Au-Cu_2O hierarchical catalyst at 150°C. Under illumination, the propylene conversion increased approximately 18-fold more than that obtained using the purely thermal

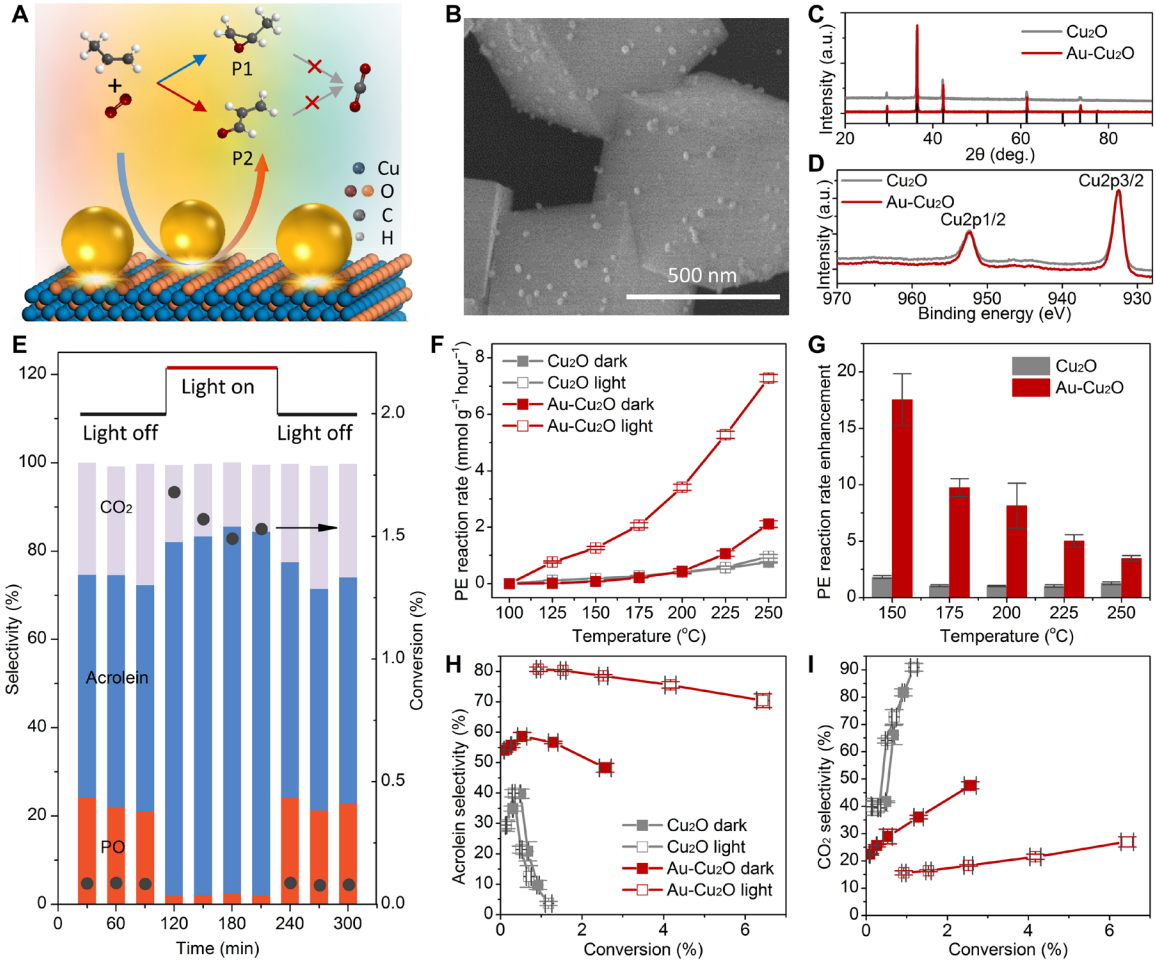

Fig. 1. Characterization of Au-Cu_2O catalyst and its catalytic performance response to illumination. (**A**) Schematic of the SP-regulated partial oxidation of propylene on the Au-Cu_2O plasmonic structure. (**B**) SEM image of the as-prepared Au-Cu_2O hierarchical structure. (**C**) XRD patterns of the as-prepared C-Cu_2O and Au-Cu_2O hierarchical structure. a.u., arbitrary unit. (**D**) XPS of Cu of the as-prepared C-Cu_2O and Au-Cu_2O hierarchical structure. (**E**) Conversion and selectivity of the partial propylene oxidation for Au-Cu_2O at 150°C with and without illumination, showing the improvement in conversion induced by light and the influence on product selectivity. (**F**) Conversion of propylene for Cu_2O and Au-Cu_2O with and without illumination at various temperatures. (**G**) Conversion enhancements induced by illumination for Cu_2O and Au-Cu_2O as a function of the operating temperature. (**H**) Selectivity of acrolein catalyzed by Cu_2O (gray) and Au-Cu_2O (red) with and without illumination as a function of propylene conversion. (**I**) Selectivity of CO_2 for Cu_2O (gray) and Au-Cu_2O (red) with and without illumination as a function of propylene conversion.

process (from 0.08 to 1.5%); concurrently, the selectivity of acrolein increased from approximately 50 to 80%. Moreover, overoxidation was inhibited, and PO formation was suppressed. Clearly, the improved catalytic performance, both conversion and selectivity, was in response to the illumination of the catalyst.

The catalytic experiment was carried out at various temperatures with and without illumination (figs. S15 to S26). As shown in Fig. 1F, in the absence of illumination, the measured reaction rate of propylene on C-Cu_2O is consistent with previous reports under similar condition (*39*). In addition, there was no measurable response to illuminating C-Cu_2O. However, on illuminating Au-Cu_2O, the propylene conversion increased greatly. Approximately 1% propylene conversion was achieved at 125°C with no external energy inputs other than photons. In contrast, without illumination, no obvious reaction took place on Cu_2O and Au-Cu_2O at 125°C. We therefore attribute this improvement to light absorption by SPs. The plasmonic enhancement can be determined by dividing the property of the same catalyst under illumination by that without illumination. As shown in Fig. 1G, no obvious enhancement was found for the C-Cu_2O. While for the hierarchical catalyst, the conversion of propylene is greatly enhanced. The enhancement decreases with the increasing temperature, similar to previous report (*29*). Using propylene conversion as criterion, the illuminated Au-Cu_2O achieved conversions comparable to those obtained on the same catalysts thermally but at temperatures approximately 75 K lower.

Figure 1H shows the selectivity of acrolein as a function of the propylene conversion with and without illumination. With C-Cu_2O, the best acrolein selectivity achieved was ~40% with ~0.5% propylene conversion. The acrolein selectivity almost did not change under illumination and quickly decreased to less than 5% when the conversion increased to 1%. With the Au-Cu_2O, there was an improvement of acrolein selectivity. Such catalytic property change of a semiconductor with adding metal NPs was attributed to the charge transfer due to the difference of their Fermi level (*42*, *43*). Moreover, the acrolein selectivity was further improved from 60 to 80% with a sixfold conversion enhancement under illumination, and the selectivity remained high despite the high conversion. In addition, an obvious inhibiting effect of the overoxidation processes was observed under illumination (Fig. 1I). For the C-Cu_2O, the main product was CO_2 (~ 90%) when the propylene conversion increased to ~1%. In contrast, the Au-Cu_2O hierarchical structure greatly reduced overoxidation under illumination, with inhibition of CO_2 selectivity to less than 30% with ~7% propylene conversion. In summary, illumination of C-Cu_2O has no beneficial effect on selective propylene oxidation. However, the excitation of SPs, made possible by using the hierarchical catalyst, improved both conversion rate and selectivity when the catalyst was illuminated with visible light. Thus, we can exclude the effect of enhanced electromagnetic field induced by SPs, which influences the chemical reaction through exciting Cu_2O. Also, we carried out the catalytic experiment with Au NPs supported on TiO_2, which is transparent in the visible regime (fig. S27). The obvious improvement of conversion and change of selectivity under illumination further proved this conclusion. Moreover, taking both the conversion and selectivity into consideration, it was impossible to achieve, simultaneously, by increasing the reaction temperature alone.

Light intensity– and wavelength-dependent experiments

Figure 2A shows the catalytic performance as a function of light intensity, in which the conversion responds supralinearly. Such supralinear dependence has been suggested as a hallmark of the chemical reaction driven by SP-induced energetic electrons (*11*, *14*, *31*). However, in the complex system with both the energetic electrons and local heating effects depending on the SP-enhanced local electromagnetic field, it is difficult to use this as sufficient evidence to determine the energetic electron process (*8*). When the light intensity increased from 100 to 500 mW/cm^2, the PE reaction rate increased from 1 to 4 mmol g^{-1} $hour^{-1}$, while the acrolein selectivity remained well at about 80%. There is a slight decrease in acrolein selectivity at 500 mW/cm^2 due to the increase in overoxidation. As shown in Fig. 2B, both the conversion and selectivity respond to the wavelength of incident light. By controlling the lamp power, the filtered light intensities of different wavelength were all 20 mW/cm^2 (fig. S28). The propylene conversion and acrolein selectivity closely tracked the extinction spectrum of the gold NPs (the red line in Fig. 2B); 550-nm incident light produced the most favorable effect, with a threefold conversion enhancement and 90% acrolein selectivity. At the same time, overoxidation and PO were inhibited. Note that the PO selectivity showed a slight increase when illuminated with 450- and 500-nm light, which was also confirmed by the enhancement ratio of the PO formation rate (fig. S29). As generally understood, the production of energetic electrons and local heating by SPs depend largely on the wavelength of the incident light (*8*, *27*, *44*). For the incident light of wavelengths shorter than 500 nm

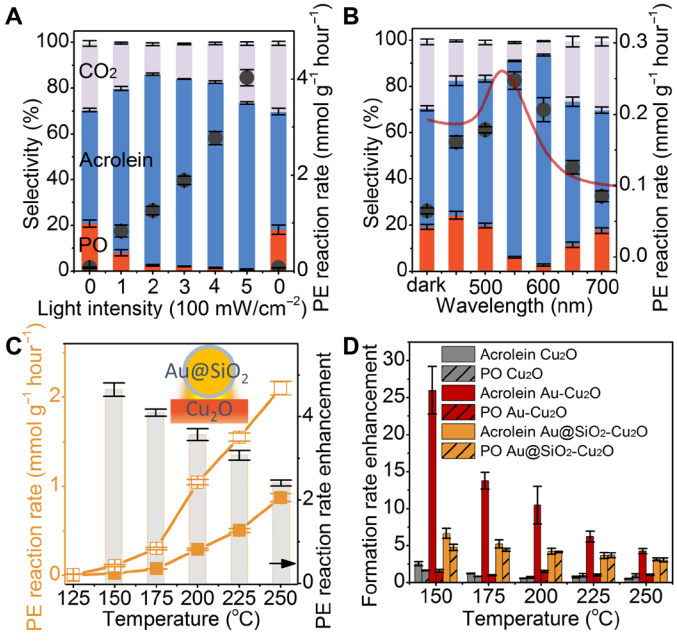

Fig. 2. The light intensity– and wavelength-dependent experiments and the catalytic performance of Au@SiO_2-Cu_2O catalyst. (**A**) Catalytic performance (conversion and selectivity) for the Au-Cu_2O hierarchical structure at 150°C as a function of incident light intensity. (**B**) Catalytic performance (conversion and selectivity) for the Au-Cu_2O hierarchical structure at 150°C as a function of incident light wavelength. The red curve is the extinction spectrum of Au NPs. (**C**) Conversion and conversion enhancement for the Au@SiO_2-Cu_2O hierarchical structure with and without illumination at various temperatures. (**D**) Formation rate enhancement of acrolein and PO as a function of temperature using Cu_2O, Au-Cu_2O hierarchical structure and Au@SiO_2-Cu_2O hierarchical structure as catalyst, calculated by dividing the formation rate of acrolein or PO with illumination by that without illumination.

(interband transition region), the excited electrons are mainly created in the vicinity of the Fermi level (i.e., with low energies), which quickly thermalize inducing local heating effect. In contrast, under SP resonant excitation, energetic electrons are efficiently generated following the decay of SPs (*45*). These suggest that the unique PO selectivity dependence on the wavelength of the incident light may result from the varying relative contributions of local heating versus energetic electrons. Similar results at 200°C are shown in fig. S30.

Distinguish energetic electrons and local heating effects

To separate energetic electrons from local heating in plasmonic catalysis, we coated the gold NPs with 5-nm-thick silica shells, which reduce electron transfer while allowing local heating (figs. S4 to S14) (*22*). Transmission electron microscopy (TEM) image, cyclic voltammetry, and Raman spectra of pyridine prove that there are no obvious pinholes in the shell (figs. S4, S31, and S32). Also, photocurrent experiments of Au@SiO_2 NPs with different thickness shells further confirm that the charge transfer process is greatly inhibited by the 5-nm SiO_2 shell (fig. S33). By using Au@SiO_2-Cu_2O hierarchical structure as catalyst, the catalytic experiment was carried out at various temperatures with and without illumination (figs. S34 to S39). In the absence of illumination, the selectivity as a function of conversion of Au@SiO_2-Cu_2O is similar to that of Cu_2O, compared with Au-Cu_2O, which confirms the validity of this strategy (figs. S40 and S41). The slight residual difference may be due to the inability to completely avoid the charge transfer process or the residue of sodium silicate. With illumination, an obvious conversion enhancement is observed, but much smaller than that for the Au-Cu_2O system, which confirms that both the energetic electrons and local heating are contributors (Fig. 2C and fig. S42). In addition, acrolein formation is improved, and overoxidation is inhibited under illumination with either Au or Au@SiO_2 NPs. However, for Au@SiO_2-Cu_2O, the PO formation rate increased about fivefold, like that for acrolein (Fig. 2D). In contrast, for Au-Cu_2O, no enhancement of the PO formation is observed; if anything, there is a small decrease (fig. S43). Combined with the wavelength-dependent results, we conclude that the local heating introduced by the SPs inhibits overoxidation, thus increasing selectivity for all partial oxidation products. This is another feature that cannot be achieved using the conventional thermal processes in a uniform thermal field.

To confirm the existence of the nanoconfined thermal fields, we calculated the temperature distribution using the conventional macroscopic model (details are given in the "Theoretical section" in the Supplementary Materials and figs. S44 to S48). Two things are taken into consideration: One is the interfacial thermal resistance between the particle and the surrounding medium, and the other is the collective heating effect related to the particle density (*46*, *47*). The thermal effect of Au NPs assembled on a Cu_2O surface with various particle densities was considered (Fig. 3). At a low particle density (25/μm^2), the high temperatures are localized in the vicinity of the particles, with limited temperature increase in the surrounding medium (Fig. 3A). Under experimental conditions, the surface particle density is in the range of 100 to 300/μm^2, as estimated from the Brunauer-Emmer-Teller (BET) surface area (1 m^2/g) and the scanning electron microscopy (SEM) images. We can safely claim that the temperature is localized for this case (Fig. 3B). At high particle densities, the temperature is no longer localized; rather, the temperature of the surrounding medium is notably increased (Fig. 3C). As shown in Fig. 3D, moderate particle densities can produce both localized

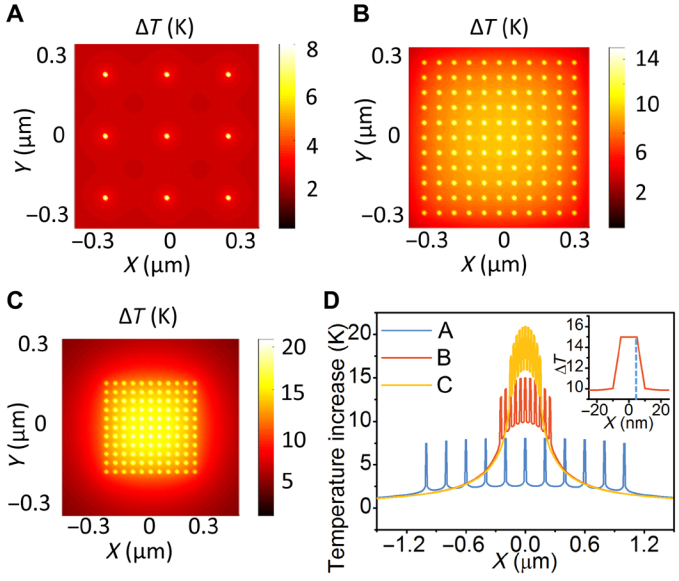

Fig. 3. The calculated heating effect with various particle concentrations. (**A**) The temperature distribution at a low surface particle density of 25/μm^2; the temperature field is localized in the vicinity of particle. (**B**) The temperature distribution with a moderate surface particle density of 300/μm^2; the temperature field is localized in the vicinity of the particle, and the collective heating effect yields a temperature rise in surrounding medium. (**C**) The temperature distribution with a high surface particle density of 1300/μm^2; the temperature is delocalized with a notable temperature increase of the surrounding medium. (**D**) Temperature distributions as a function of *X*, as shown in (A) (blue solid line), (B) (red solid line), and (C) (yellow solid line). A moderate particle density can produce a considerable localized temperature with great gradient around particles and certain temperature increase of the surrounding medium. Particle arrays (11 × 11) with various periodicities were used to simulate the particle-covered substrate surface. A section of the plane 2 nm above the substrate is used to facilitate a top view of the temperature distribution.

temperatures (over an area with ~10-nm diameter) with a considerable gradient around the particles (~1 K/nm) and an obvious temperature increase of the surrounding medium (2 to 10 K). Taking the heat released by the localized reaction into consideration, the gradient is expected to be even larger.

DISCUSSION

Hence, we conclude that the unique environment created by SPs, which can greatly enhance the conversion and regulate the selectivity of propylene-selective oxidation concurrently, is attributed to the coupling of energetic electrons with nanoconfined thermal fields. They act on the chemical reaction through differing ways, resulting in different outcomes. The proposed elementary mechanisms of the plasmon-mediated selective propylene oxidation are shown in Fig. 4. As reported, the energetic electrons can promote oxygen activation (*29*, *30*) and weaken the Cu—O bonds in surface Cu_2O (*12*). For propylene partial oxidation, the lattice oxygen as the nucleophilic oxygen species promotes acrolein formation (*3*, *41*). Thus, in the Au-Cu_2O system, the energetic electrons regulated the reaction path to improve the acrolein selectivity while decreasing the PO selectivity under illumination. In addition, Au NPs on SiO_2 showed no activity under illumination (fig. S8), which proved that energetic electrons mainly interact with oxygen species indirectly via Cu_2O (*48*). On

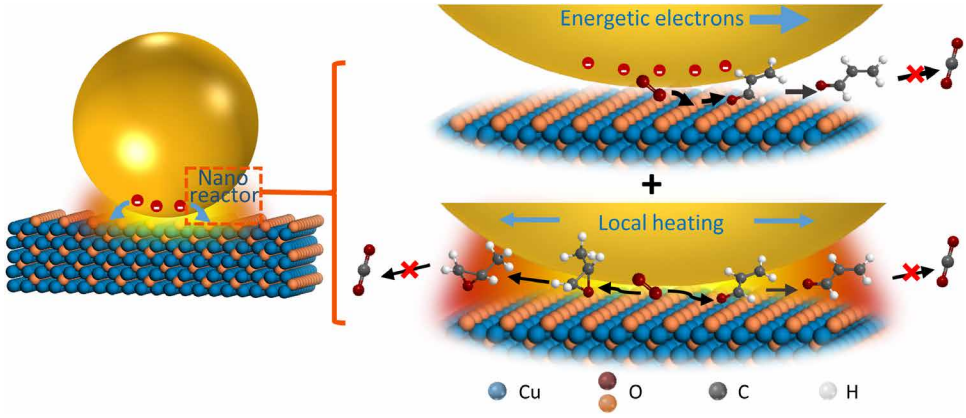

Fig. 4. Schematic of the photoelectronic and photothermal contributions to the chemical reaction. Both energetic electrons and local heating effects influence the chemical reaction but through different ways. The energetic electrons regulate the reaction path to improve the acrolein selectivity. The local heating effect of SPs in the hierarchical structure can isolate the active region to eliminate consecutive reactions, thus greatly reducing overoxidation and increasing the selectivity of all partial oxidation products.

the other hand, the thermal field created by SPs is confined to the nanoscale with a large gradient, which can increase the distribution of activated reactants to overcome the energy barriers. However, overoxidation is quickly suppressed as a result of the rapid diffusion of the partial oxidation product out of this reaction zone, which reduces consecutive reactions, thereby increasing the selectivity of both acrolein and PO. This spatial effect also holds for the localized energetic electrons, which are reported to drive chemical reactions in localized regions (*32*, *33*). In addition, the confined high-temperature region can accelerate product removal (*11*), which further reduces overoxidation. To summarize, plasmonic nanoreactors generated by confining energetic electrons and thermal fields in open space can promote conversion rate and regulate selectivity concurrently. Also, the distribution of the energetic electrons and thermal fields in these nanoreactors are inhomogeneous with great gradient. The nanoconfined thermal fields inhibit overoxidation, thus increasing selectivity of all partial oxidation products. However, energetic electrons can regulate the reaction pathway, which is very unlikely to be achieved by just increasing temperature, thus selectively promoting the formation of acrolein.

In this work, we show that the plasmonic reactor can couple energetic electrons and nanoconfined thermal fields concurrently, thereby promoting conversion rate and regulating selectivity concurrently rather than competitively. Moreover, the plasmonic reactors have different effects on chemical reactions: regulation of the reaction pathway and reduction of consecutive reactions to greatly reduce overoxidation. Through judicious design, plasmonic nanostructures can be made to mutually affect selectivity and efficiency, suggesting a paradigm that can be applied to a range of catalytic process with branching ratios, leading alternately to desirable and undesirable products. In summary, surface plasmons offer new mechanistic possibilities for carrying out catalytic reactions, enabling the more efficient use of solar energy to drive chemical transformations.

MATERIALS AND METHODS

Synthesis of C-Cu_2O

$Cu(NO_3)_2{\cdot}3H_2O$ (2 mmol) was dissolved into 20 ml of water in a glass vial, then 6 ml of 1 M NaOH was added with vigorous stirring for 5 min in a water bath at 60°C. Last, 6 ml of 1 M D-(+)-glucose was introduced as a reductant, and the reaction was kept for 1 hour in the bath. The color of the solution gradually turned from deep blue into yellow. When the reaction was finished, the precipitate was separated from the solution by centrifugation at 3000 revolutions per minute (rpm) for 3 min, washed several times with ethanol, and, lastly, dried under vacuum at ambient temperature.

Synthesis of Au NPs and Au@SiO_2 NPs

The 30-nm Au NPs were synthesized by reducing the boiling 0.01% weight (wt) % $HAuCl_4{\cdot}4H_2O$ (100 ml) with 1 wt % sodium citrate solution (1.2 ml) under a vigorous stirring (*49*). The Au@SiO_2 NPs were prepared by coating the silica onto 30-nm Au NPs via the hydrolysis of sodium silicate in 90°C water. (3-Aminopropyl)trimethoxysilane (1 mM) aqueous solution was added to the gold sol under vigorous magnetic stirring in 15 min to ensure complexation of the amine groups with the gold surface. Then, a 0.54 wt % sodium silicate solution was added to the sol, again under vigorous magnetic stirring. The thickness of the silica shell was controlled by the hydrolysis time. The Au@SiO_2 NPs that we used with a 5-nm SiO_2 shell were hydrolyzed for 1.5 hours (*50*).

Synthesis of the catalyst Au-Cu_2O and Au@SiO_2-Cu_2O

The Au-Cu_2O heterostructure was assembled using as-prepared Au NPs and cube Cu_2O nanocrystals. The gold sol (100 ml) was centrifuged for several times and transferred to ethyl alcohol, and then injected into the well-dispersed C-Cu_2O (470 mg) sol to complete the assembly process. After shaking for 30 min, the precipitate was separated from the solution by centrifugation at 3000 rpm for 3 min, washed with ethanol, and, lastly, dried under vacuum at ambient temperature. The Au@SiO_2-Cu_2O catalyst was prepared with similar processes but using as-prepared Au@SiO_2 NPs and cube Cu_2O nanocrystals as components.

Synthesis of the catalyst Au-SiO_2

A known amount of support material, SiO_2 (surface area ~80 to 100 m^2/g), was added under stirring to the gold sol, which had been cleaned and transferred to ethanol to prepare catalyst with final composition of 1 wt % Au/SiO_2. The catalyst was further washed

with ethanol by centrifugation and dried in nitrogen at room temperature.

Characterization of samples

The composition and phase of all the as-prepared products were detected by a Rigaku Ultima IV x-ray diffractometer, which operated at a voltage of 35 kV and a current of 15 mA with Cu-K_α radiation. SEM (S4800) was used to observe the size and morphology of the as-prepared products. TEM images were taken by a JEM-2100 high-resolution transmission electron microscope (JEOL, Tokyo, Japan) with an acceleration voltage of 200 kV. All TEM samples were prepared by depositing a drop of diluted suspensions in ethanol on a carbon film–coated copper grid, followed by drying under infrared light. Surface area of samples was carried out with a BET model by Micromeritics TriStar 3020 and porosimetry analyzer at 77 K, where samples were pretreated at 473 K in vacuum for 3 hours before N_2 adsorption measurements. The ultraviolet-visible (UV-vis) absorption spectrum was carried out by the Cary 5000 with the Integrating sphere model (Agilent). The XPS was carried out by using a Physical Electronics Quantum 2000 photoelectron spectrometer (Al K_α with 1486.6 eV, operating at 15 kV, 35 W, and 200-μm spot size) and an Omicron Sphera II hemispherical electron energy analyzer (monochromatic Al Kα with 1486.6 eV, operating at 15 kV and 300 W). The base pressure of the systems was 5.0×10^{-9} mbar. The samples were pressed into a pellet for the XPS measurements. The UV-vis absorption spectrum was acquired by the Cary 5000 (Agilent) with the Integrating sphere mode for powder samples and transmission mode for liquid samples.

Catalytic experiments

Catalytic reactions were carried out in a fixed-bed quartz reactor with a vertically oriented squashed window (0.1 cm × 2 cm^2) to allow illumination. The experiments were operated under atmospheric pressure. The reactant gas mixture (the rate of helium/C_3H_6/O_2 is 40:13.3:6.7) with a flow rate of 50 ml·min^{-1} was introduced into the reactor to start the reaction. Different temperature points (from 100° to 250°C) were established to measure the catalytic performance of the as-prepared catalysts. The temperature was measured by a thermocouple, corresponding to ambient temperature. Catalyst (200 mg) was used each time and heated to the setting temperature at 5°C·min^{-1}. The reaction products were analyzed by online gas chromatographs equipped with two columns. PO, acrolein, allyl alcohol, propanal, acetone, and acetaldehyde were separated by a free fatty acid phase capillary column (FFAP, 50 m × 0.53 mm × 1.0 μm) and detected by flame ionization detector. Other components, such as O_2, C_3H_6, and CO_2, were separated by Porapak Q and detected thermal conductivity detectors. All the lines and valves between the exit of the reactor and the gas chromatographs were heated to 393 K to prevent condensation of organic products. The light intensity for the catalytic experiment with illumination at different temperature is 200 mW/cm^2. To study the impact of light switching, light intensity, and wavelength, the light switching–, light intensity–, and wavelength-dependent experiments were carried out at constant temperature (150°C). For the light switching experiments, the incident light intensity was 200 mW/cm^2. For the light intensity–dependent experiments, the source intensity was adjusted from 100 to 500 mW/cm^2 by controlling the power to the source. The wavelength-dependent experiments were performed using a series of band-pass filters. For these experiments, at constant temperature, the system was allowed 20 min to reach steady state.

Theoretical calculation of the electromagnetic field and thermal field

The simulation of electromagnetic fields is performed using the commercial finite elements method software COMSOL Multiphysics. To avoid numerical difficulties, as widely applied in the literature, a small gap (~1 nm) is introduced to relax the mesh singularities (*51*). Since the substrate is a semiconductor, the NPs are weakly coupled with the substrates. Introducing small gaps will not affect the optical response of the studied system. The photothermal effect and temperature distribution are analyzed using the conventional macroscopic model, which is described by the usual heat transfer equation (*52*): $\rho c\frac{\partial T}{\partial t} = \nabla \cdot (k\nabla T) + Q_0$, where T is the local temperature increase, ρ is the mass density, c is the heat capacity, and k is the thermal conductivity. The local heat source density Q_0 origins from the nonradiative energy damping in gold NPs, which writes as $Q_0 = \frac{1}{2}\omega\varepsilon_0\varepsilon_{au}^{``}|E_\omega|^2$, where ω is the angular frequency of incident photon, $\varepsilon_0$ is the vacuum permittivity, $\varepsilon_{au}^{``}$ is the imaginary part of the relative permittivity of gold adopted from Johnson and Christy's experimental data (*53*), and E_ω is the local electric field derived from electromagnetic simulations. In the experimental condition, the illumination time is in tens of minutes, which is much longer than thermal relaxation times; therefore, the equation can be simplified as the Poisson's equation: $\nabla^2 T = -\frac{Q_0}{k}$. In homogeneous medium, the stationary solutions of the equation involve the thermal Green's function and a Dirac source inside particles (*46*).

SUPPLEMENTARY MATERIALS

Supplementary material for this article is available at http://advances.sciencemag.org/cgi/content/full/7/10/eabf0962/DC1

REFERENCES AND NOTES

1. B. Hammer, J. K. Norskov, Why gold is the noblest of all the metals. *Nature* **376**, 238–240 (1995).
2. A. Wittstock, V. Zielasek, J. Biener, C. M. Friend, M. Bäumer, Nanoporous gold catalysts for selective gas-phase oxidative coupling of methanol at low temperature. *Science* **327**, 319–322 (2010).
3. J. Huang, M. Haruta, Gas-phase propene epoxidation over coinage metal catalysts. *Res. Chem. Intermed.* **38**, 1–24 (2012).
4. E. C. Tyo, S. Vajda, Catalysis by clusters with precise numbers of atoms. *Nat. Nano.* **10**, 577–588 (2015).
5. C. T. Campbell, S. C. Parker, D. E. Starr, The effect of size-dependent nanoparticle energetics on catalyst sintering. *Science* **298**, 811–814 (2002).
6. J. A. Schuller, E. S. Barnard, W. Cai, Y. C. Jun, J. S. White, M. L. Brongersma, Plasmonics for extreme light concentration and manipulation. *Nat. Mater.* **9**, 193–204 (2010).
7. J. J. Baumberg, J. Aizpurua, M. H. Mikkelsen, D. R. Smith, Extreme nanophotonics from ultrathin metallic gaps. *Nat. Mater.* **18**, 668–678 (2019).
8. C. Zhan, X.-J. Chen, J. Yi, J.-F. Li, D.-Y. Wu, Z.-Q. Tian, From plasmon-enhanced molecular spectroscopy to plasmon-mediated chemical reactions. *Nat. Rev. Chem.* **2**, 216–230 (2018).
9. F. Neubrech, X. Duan, N. Liu, Dynamic plasmonic color generation enabled by functional materials. *Sci. Adv.* **6**, eabc2709 (2020).
10. S. Mubeen, J. Lee, N. Singh, S. Kramer, G. D. Stucky, M. Moskovits, An autonomous photosynthetic device in which all charge carriers derive from surface plasmons. *Nat. Nanotech.* **8**, 247–251 (2013).
11. D. F. Swearer, H. Zhao, L. Zhou, C. Zhang, H. Robatjazi, J. M. P. Martirez, C. M. Krauter, S. Yazdi, M. J. McClain, E. Ringe, E. A. Carter, P. Nordlander, N. J. Halas, Heterometallic antenna–reactor complexes for photocatalysis. *Proc. Nat. Acad. Sci. U.S.A.* **113**, 8916–8920 (2016).
12. A. Marimuthu, J. Zhang, S. Linic, Tuning selectivity in propylene epoxidation by plasmon mediated photo-switching of Cu oxidation state. *Science* **339**, 1590–1593 (2013).
13. L. Zhou, D. F. Swearer, C. Zhang, H. Robatjazi, H. Zhao, L. Henderson, L. Dong, P. Christopher, E. A. Carter, P. Nordlander, N. J. Halas, Quantifying hot carrier and thermal contributions in plasmonic photocatalysis. *Science* **362**, 69–72 (2018).
14. Y. Kim, J. G. Smith, P. K. Jain, Harvesting multiple electron–hole pairs generated through plasmonic excitation of Au nanoparticles. *Nat. Chem.* **10**, 763–769 (2018).
15. T. Oshikiri, K. Ueno, H. Misawa, Plasmon-induced ammonia synthesis through nitrogen photofixation with visible light irradiation. *Angew. Chem. Int. Ed.* **53**, 9802–9805 (2014).

16. C. Zhan, Z.-Y. Wang, X.-G. Zhang, X.-J. Chen, Y.-F. Huang, S. Hu, J.-F. Li, D.-Y. Wu, M. Moskovits, Z.-Q. Tian, Interfacial construction of plasmonic nanostructures for the utilization of the plasmon-excited electrons and holes. *J. Am. Chem. Soc.* **141**, 8053–8057 (2019).
17. A. Tittl, X. Yin, H. Giessen, X.-D. Tian, Z.-Q. Tian, C. Kremers, D. N. Chigrin, N. Liu, Plasmonic smart dust for probing local chemical reactions. *Nano Lett.* **13**, 1816–1821 (2013).
18. B. Munkhbat, M. Wersäll, D. G. Baranov, T. J. Antosiewicz, T. Shegai, Suppression of photo-oxidation of organic chromophores by strong coupling to plasmonic nanoantennas. *Sci. Adv.* **4**, eaas9552 (2018).
19. C. Clavero, Plasmon-induced hot-electron generation at nanoparticle/metal-oxide interfaces for photovoltaic and photocatalytic devices. *Nat. Photonics* **8**, 95–103 (2014).
20. M. L. Brongersma, N. J. Halas, P. Nordlander, Plasmon-induced hot carrier science and technology. *Nat. Nanotech.* **10**, 25–34 (2015).
21. P. Christopher, M. Moskovits, Hot charge carrier transmission from plasmonic nanostructures. *Annu. Rev. Phys. Chem.* **68**, 379–398 (2017).
22. J. Li, S. K. Cushing, F. Meng, T. R. Senty, A. D. Bristow, N. Wu, Plasmon-induced resonance energy transfer for solar energy conversion. *Nat. Photonics* **9**, 601–607 (2015).
23. J. J. Baumberg, Hot electron science in plasmonics and catalysis: What we argue about. *Faraday Discuss.* **214**, 501–511 (2019).
24. J. S. DuChene, G. Tagliabue, A. J. Welch, W.-H. Cheng, H. A. Atwater, Hot hole collection and photoelectrochemical CO_2 reduction with plasmonic Au/p-GaN photocathodes. *Nano Lett.* **18**, 2545–2550 (2018).
25. S. Linic, U. Aslam, C. Boerigter, M. Morabito, Photochemical transformations on plasmonic metal nanoparticles. *Nat. Mater.* **14**, 567–576 (2015).
26. U. Aslam, V. G. Rao, S. Chavez, S. Linic, Catalytic conversion of solar to chemical energy on plasmonic metal nanostructures. *Nat. Catal.* **1**, 656–665 (2018).
27. Y. Zhang, S. He, W. Guo, Y. Hu, J. Huang, J. R. Mulcahy, W. D. Wei, Surface-plasmon-driven hot electron photochemistry. *Chem. Rev.* **118**, 2927–2954 (2018).
28. G. Baffou, R. Quidant, Nanoplasmonics for chemistry. *Chem. Soc. Rev.* **43**, 3898–3907 (2014).
29. P. Christopher, H. Xin, S. Linic, Visible-light-enhanced catalytic oxidation reactions on plasmonic silver nanostructures. *Nat. Chem.* **3**, 467–472 (2011).
30. Y.-F. Huang, M. Zhang, L.-B. Zhao, J.-M. Feng, D.-Y. Wu, B. Ren, Z.-Q. Tian, Activation of oxygen on gold and silver nanoparticles assisted by surface plasmon resonances. *Angew. Chem. Int. Ed.* **53**, 2353–2357 (2014).
31. P. Christopher, H. Xin, A. Marimuthu, S. Linic, Singular characteristics and unique chemical bond activation mechanisms of photocatalytic reactions on plasmonic nanostructures. *Nat. Mater.* **11**, 1044–1050 (2012).
32. E. Cortés, W. Xie, J. Cambiasso, A. S. Jermyn, R. Sundararaman, P. Narang, S. Schlücker, S. A. Maier, Plasmonic hot electron transport drives nano-localized chemistry. *Nat. Commun.* **8**, 14880 (2017).
33. E. Kazuma, J. Jung, H. Ueba, M. Trenary, Y. Kim, Real-space and real-time observation of a plasmon-induced chemical reaction of a single molecule. *Science* **360**, 521–526 (2018).
34. W.-C. D. Yang, C. Wang, L. A. Fredin, P. A. Lin, L. Shimomoto, H. J. Lezec, R. Sharma, Site-selective CO disproportionation mediated by localized surface plasmon resonance excited by electron beam. *Nat. Mater.* **18**, 614–619 (2019).
35. U. Aslam, S. Chavez, S. Linic, Controlling energy flow in multimetallic nanostructures for plasmonic catalysis. *Nat. Nanotech.* **12**, 1000–1005 (2017).
36. L. Zhou, J. M. P. Martirez, J. Finzel, C. Zhang, D. F. Swearer, S. Tian, H. Robatjazi, M. Lou, L. Dong, L. Henderson, P. Christopher, E. A. Carter, P. Nordlander, N. J. Halas, Light-driven methane dry reforming with single atomic site antenna-reactor plasmonic photocatalysts. *Nat. Energy* **5**, 61–70 (2020).
37. D. Torres, N. Lopez, F. Illas, R. M. Lambert, Low-basicity oxygen atoms: A key in the search for propylene epoxidation catalysts. *Angew. Chem. Int. Ed.* **46**, 2055–2058 (2007).
38. W. Zhu, Q. Zhang, Y. Wang, Cu(I)-catalyzed epoxidation of propylene by molecular oxygen. *J. Phys. Chem. C* **112**, 7731–7734 (2008).
39. Q. Hua, T. Cao, X.-K. Gu, J. Lu, Z. Jiang, X. Pan, L. Luo, W.-X. Li, W. Huang, Crystal-plane-controlled selectivity of Cu_2O catalysts in propylene oxidation with molecular oxygen. *Angew. Chem. Int. Ed.* **53**, 4856–4861 (2014).
40. R. L. Myers, *The 100 Most Important Chemical Compounds* (Greenwood Press, 2007).
41. Y. Wang, H. Chu, W. Zhu, Q. Zhang, Copper-based efficient catalysts for propylene epoxidation by molecular oxygen. *Catal. Today* **131**, 496–504 (2008).
42. G. Schwab, K. Koller, Combined action of metal and semiconductor catalysts. *J. Am. Chem. Soc.* **90**, 3078–3080 (1968).
43. J. Y. Park, L. R. Baker, G. A. Somorjai, Role of hot electrons and metal–oxide interfaces in surface chemistry and catalytic reactions. *Chem. Rev.* **115**, 2781–2817 (2015).
44. E. Pensa, J. Gargiulo, A. Lauri, S. Schlücker, E. Cortés, S. A. Maier, Spectral screening of the energy of hot holes over a particle plasmon resonance. *Nano Lett.* **19**, 1867–1874 (2019).
45. B. Y. Zheng, H. Zhao, A. Manjavacas, M. McClain, P. Nordlander, N. J. Halas, Distinguishing between plasmon-induced and photoexcited carriers in a device geometry. *Nat. Commun.* **6**, 7797 (2015).
46. G. Baffou, R. Quidant, C. Girard, Thermoplasmonics modeling: A Green's function approach. *Phys. Rev. B* **82**, 165424 (2010).
47. N. J. Hogan, A. S. Urban, C. Ayala-Orozco, A. Pimpinelli, P. Nordlander, N. J. Halas, Nanoparticles heat through light localization. *Nano Lett.* **14**, 4640–4645 (2014).
48. H. Robatjazi, H. Zhao, D. F. Swearer, N. J. Hogan, L. Zhou, A. Alabastri, M. J. McClain, P. Nordlander, N. J. Halas, Plasmon-induced selective carbon dioxide conversion on earth-abundant aluminum-cuprous oxide antenna-reactor nanoparticles. *Nat. Commun.* **8**, 27 (2017).
49. G. Frens, Controlled nucleation for the regulation of the particle size in monodisperse gold suspensions. *Nat. Phys. Sci.* **241**, 20–22 (1973).
50. J. F. Li, Y. F. Huang, Y. Ding, Z. L. Yang, S. B. Li, X. S. Zhou, F. R. Fan, W. Zhang, Z. Y. Zhou, D. Y. Wu, B. Ren, Z. L. Wang, Z. Q. Tian, Shell-isolated nanoparticle-enhanced Raman spectroscopy. *Nature* **464**, 392–395 (2010).
51. J. Wen, H. Wang, W. Wang, Z. Deng, C. Zhuang, Y. Zhang, F. Liu, J. She, J. Chen, H. Chen, S. Deng, N. Xu, Room-temperature strong light–matter interaction with active control in single plasmonic nanorod coupled with two-dimensional atomic crystals. *Nano Lett.* **17**, 4689–4697 (2017).
52. A. O. Govorov, W. Zhang, T. Skeini, H. Richardson, J. Lee, N. A. Kotov, Gold nanoparticle ensembles as heaters and actuators: Melting and collective plasmon resonances. *Nano. Res. Lett.* **1**, 84–90 (2006).
53. P. B. Johnson, R. W. Christy, Optical constants of the noble metals. *Phys. Rev. B* **6**, 4370–4379 (1972).
54. J. Ghijsen, L. H. Tjeng, J. van Elp, H. Eskes, J. Westerink, G. A. Sawatzky, M. T. Czyzyk, Electronic structure of Cu_2O and CuO. *Phys. Rev. B* **38**, 11322–11330 (1988).
55. S. Poulston, P. M. Parlett, P. Stone, M. Bowker, Surface oxidation and reduction of CuO and Cu2O studied using XPS and XAES. *Surf. Interface Anal.* **24**, 811–820 (1996).
56. N. Kruse, S. Chenakin, XPS characterization of Au/TiO_2 catalysts: Binding energy assessment and irradiation effects. *Appl. Catal. A* **391**, 367–376 (2011).
57. I. Tunc, S. Suzer, M. A. Correa-Duarte, L. M. Liz-Marzán, XPS characterization of Au (core)/ SiO2 (shell) nanoparticles. *J. Phys. Chem. B* **109**, 7597–7600 (2005).
58. C. Zhan, B.-W. Liu, Y.-F. Huang, S. Hu, B. Ren, M. Moskovits, Z.-Q. Tian, Disentangling charge carrier from photothermal effects in plasmonic metal nanostructures. *Nat. Commun.* **10**, 2671 (2019).
59. E. D. Palik, *Handbook of Optical Constants of Solids* (Academic press, 1998), vol. 3.
60. H. Ghasemi, G. Ni, A. M. Marconnet, J. Loomis, S. Yerci, N. Miljkovic, G. Chen, Solar steam generation by heat localization. *Nat. Commun.* **5**, 4449 (2014).
61. O. Neumann, A. S. Urban, J. Day, S. Lal, P. Nordlander, N. J. Halas, Solar vapor generation enabled by nanoparticles. *ACS Nano* **7**, 42–49 (2013).
62. J. Alpert, K. Hamad-Schifferli, Effect of ligands on thermal dissipation from gold nanorods. *Langmuir* **26**, 3786–3789 (2010).
63. J. A. Eastman, S. R. Phillpot, S. U. S. Choi, P. Keblinski, Thermal transport in nanofluids. *Annu. Rev. Mater. Chem.* **34**, 219–246 (2004).
64. H. H. Richardson, M. T. Carlson, P. J. Tandler, P. Hernandez, A. O. Govorov, Experimental and theoretical studies of light-to-heat conversion and collective heating effects in metal nanoparticle solutions. *Nano Lett.* **9**, 1139–1146 (2009).
65. G. Baffou, P. Berto, E. Bermúdez Ureña, R. Quidant, S. Monneret, J. Polleux, H. Rigneault, Photoinduced heating of nanoparticle arrays. *ACS Nano* **7**, 6478–6488 (2013).

Acknowledgments: We thank J.-F. Li, G. Fu, Q. Kuang, Q.-H. Zhang, X. Jin, and L.-Y. Zhou for helpful discussions. **Funding:** We acknowledge support from the Ministry of Science and Technology of China (2015CB932300), the National Natural Science Foundation of China (21533006 and 91427304), and the 111 Project of China (B08027 and B17027). **Author contributions:** Z.-Q.T., Z.-X.X., and M.M. supervised the project. C.Z. conceived the ideas. C.Z. and Q.-X.W. performed the experiments. J.Y. performed the calculation of thermal field. L.C. helped with the characterization of catalysts. C.Z. wrote the first draft of paper. C.Z., Q.-X.W, J.Y., L.C., D.-Y.W., Y.W., Z.-X.X., M.M., and Z.-Q.T. contributed to the data interpretation and edited the manuscript. M.M., Z.-Q.T., and Z.-X.X. revised the manuscript before the final submission. **Competing interests:** The authors declare that they have no competing interests. **Data and materials availability:** All data needed to evaluate the conclusions in the paper are present in the paper and/or the Supplementary Materials. Additional data related to this paper may be requested from the authors.

Submitted 3 October 2020
Accepted 21 January 2021
Published 5 March 2021
10.1126/sciadv.abf0962

Citation: C. Zhan, Q.-X. Wang, J. Yi, L. Chen, D.-Y. Wu, Y. Wang, Z.-X. Xie, M. Moskovits, Z.-Q. Tian, Plasmonic nanoreactors regulating selective oxidation by energetic electrons and nanoconfined thermal fields. *Sci. Adv.* **7**, eabf0962 (2021).